A Comparison of FDTD-PML With TDIE

Niraj Sachdeva, Sadasiva M. Rao, *Fellow, IEEE*, and N. Balakrishnan

***Abstract*—Presented in this paper, is a comparison of two popular numerical techniques, *viz.* the finite-difference time-domain method and the time domain integral equation method, for electromagnetic-scattering problems. The comparison is made via standard canonical shapes, a cube, and a sphere, to address the factors affecting accuracy, efficiency, and the required computer resources.**

***Index Terms*—Differential equations, finite-difference methods, integral equations, method of moments (MoM).**

I. Introduction

In this work, we present a comparison of two popular and widely different numerical methods, *viz.* the finite-difference time-domain (FDTD) method [1] and the time domain integral equation (TDIE) method [2]. However, we restrict our comparison to open region problems only, in particular, the far-field calculations. As is well known, the FDTD method is a differential equation based technique used for solving electromagnetic wave interaction problems for open as well as closed regions. When applied to open region problems, FDTD requires a suitable absorbing boundary condition. At present, the most popular and accurate boundary condition seems to be the perfectly matched layer (PML) [3], [4]. On the other hand, as the name implies, TDIE is an integral equation based technique which incorporates radiation condition in the formulation itself. To the best of our knowledge, a thorough comparison of these two techniques has not been made and this work is aimed at filling this gap. It is also hoped that this comparison might help in choosing one method over the other for a given situation.

This paper is organized as follows. In the next two sections, for the sake of completeness, we present a brief description of TDIE and FDTD with the PML boundary methods, respectively. In Section IV, numerical results are presented to show the comparison between these two methods. Finally, in Section V, we present the conclusions drawn from this study.

II. Formulation of TDIE

Consider an arbitrarily shaped, dielectric body described by a surface S. The scatterer has material parameters of μ_d and ϵ_d while exterior to the body is a homogeneous medium with parameters μ_e and ϵ_e. Exterior to the body, the total fields are designated by $\boldsymbol{E}_e$ and $\boldsymbol{H}_e$, while interior to the object, the fields are given by $\boldsymbol{E}_d$ and $\boldsymbol{H}_d$. The structure is illuminated by an arbitrary electromagnetic, plane-wave pulse. Also, we note that the tangential components of the electric and magnetic fields must be continuous at the dielectric interface S as dictated by the boundary conditions.

Before we start the integral equation formulation, we assume that the dielectric body is a closed body so that a unique outward normal vector can be defined unambiguously. Employing the equivalence principle [5] the body may be replaced with two sets of electric ($\boldsymbol{J}_e$ and $\boldsymbol{J}_d$) and magnetic ($\boldsymbol{M}_e$ and $\boldsymbol{M}_d$) currents. Each set radiates in an infinite homogeneous medium having constitutive parameters associated with medium "e" or "d". It can be easily proved that the continuity of the tangential fields require that

$$\boldsymbol{J}_e = -\boldsymbol{J}_d \equiv \boldsymbol{J} \tag{1}$$

$$\boldsymbol{M}_e = -\boldsymbol{M}_d \equiv \boldsymbol{M}. \tag{2}$$

Using the potential theory [5], the scattered fields radiated by the equivalent electric and magnetic currents may be written in terms of potential functions as

$$\boldsymbol{E}^s_\nu[\boldsymbol{J},\boldsymbol{M}] = \mp\frac{\partial \boldsymbol{A}_\nu}{\partial t} \mp \nabla\Phi^e_\nu \mp \frac{1}{\epsilon_\nu}\nabla\times\boldsymbol{F}_\nu \tag{3}$$

$$\boldsymbol{H}^s_\nu[\boldsymbol{J},\boldsymbol{M}] = \mp\frac{\partial \boldsymbol{F}_\nu}{\partial t} \mp \nabla\Phi^m_\nu \mp \frac{(-1)}{\mu_\nu}\nabla\times\boldsymbol{A}_\nu \tag{4}$$

where $\boldsymbol{A}_\nu$ and $\boldsymbol{F}_\nu$ are the magnetic and electric vector potentials, respectively, and Φ^e_ν and Φ^m_ν are the electric and magnetic scalar potentials, respectively, given by

$$\boldsymbol{A}_\nu(\boldsymbol{r},t) = \frac{\mu_\nu}{4\pi}\int_S \frac{\boldsymbol{J}(\boldsymbol{r}', t-\frac{R}{c_\nu})}{R}\,dS' \tag{5}$$

$$\boldsymbol{F}_\nu(\boldsymbol{r},t) = \frac{\epsilon_\nu}{4\pi}\int_S \frac{\boldsymbol{M}(\boldsymbol{r}', t-\frac{R}{c_\nu})}{R}\,dS' \tag{6}$$

$$\Phi^e_\nu(\boldsymbol{r},t) = \frac{1}{4\pi\epsilon_\nu}\int_S \frac{q^e_s(\boldsymbol{r}', t-\frac{R}{c_\nu})}{R}\,dS' \tag{7}$$

$$\Phi^m_\nu(\boldsymbol{r},t) = \frac{1}{4\pi\mu_\nu}\int_S \frac{q^m_s(\boldsymbol{r}', t-\frac{R}{c_\nu})}{R}\,dS' \tag{8}$$

for $\nu = e$ or $\nu = d$ and the "$-$" sign is for $\nu = e$ and the "$+$" is for $\nu = d$. In (5)–(8), $R = |\boldsymbol{r} - \boldsymbol{r}'|$, the distance from the field point $\boldsymbol{r}$ to the source point $\boldsymbol{r}'$. The electric and magnetic surface charge density q^e_s and q^m_s, respectively, are related to the electric and magnetic surface current density by the continuity equations

$$\nabla_s\cdot\boldsymbol{J} = -\frac{\partial q^e_s}{\partial t} \tag{9}$$

$$\nabla_s\cdot\boldsymbol{M} = -\frac{\partial q^m_s}{\partial t} \tag{10}$$

Manuscript received November 23, 1999; revised March 5, 2001.

N. Sachdeva, deceased, was with the Department of Aerospace Engineering, Indian Institute of Science, Bangalore 560012, India.

N. Balakrishnan is with the Department of Aerospace Engineering, Indian Institute of Science, Bangalore 560012, India.

S. M. Rao is with the Department of Electrical and Computer Engineering, Auburn University, Auburn AL 36849 USA.

Digital Object Identifier 10.1109/TAP.2002.804024

respectively. Note that the time retardation R/c_ν depends upon which medium the field is in. We may eliminate q_s^e and q_s^m from (7) and (8), respectively, by defining

$$\Psi_\nu^e(\boldsymbol{r},t) \equiv \frac{\partial \Phi_\nu^e(\boldsymbol{r},t)}{\partial t} = \frac{1}{4\pi\epsilon_\nu}\int_S \frac{\partial q_s^e\left(\boldsymbol{r}', t-\frac{R}{c_\nu}\right)}{\partial t}\frac{1}{R}\,dS' \quad (11)$$

$$= \frac{-1}{4\pi\epsilon_\nu}\int_S \frac{\nabla_s' \cdot \boldsymbol{J}(\boldsymbol{r}', t-\frac{R}{c_\nu})}{R}\,dS' \quad (12)$$

$$\Psi_\nu^m(\boldsymbol{r},t) \equiv \frac{\partial \Phi_\nu^m(\boldsymbol{r},t)}{\partial t} = \frac{1}{4\pi\mu_\nu}\int_S \frac{\partial q_s^m(\boldsymbol{r}', t-\frac{R}{c_\nu})}{\partial t}\frac{1}{R}\,dS' \quad (13)$$

$$= \frac{-1}{4\pi\mu_\nu}\int_S \frac{\nabla_s' \cdot \boldsymbol{M}(\boldsymbol{r}', t-\frac{R}{c_\nu})}{R}\,dS'. \quad (14)$$

By enforcing the continuity of the tangential electric and magnetic fields at the dielectric interface and taking an extra derivative with respect to time, we derive the following integral equations:

$$\frac{\partial}{\partial t}\left[\boldsymbol{E}_e^s - \boldsymbol{E}_d^s\right]_{\tan} = -\frac{\partial}{\partial t}\left[\boldsymbol{E}^i\right]_{\tan} \quad \boldsymbol{r}\in S, \quad (15)$$

$$\frac{\partial}{\partial t}\left[\boldsymbol{H}_e^s - \boldsymbol{H}_d^s\right]_{\tan} = -\frac{\partial}{\partial t}\left[\boldsymbol{H}^i\right]_{\tan} \quad \boldsymbol{r}\in S \quad (16)$$

which can be rewritten as

$$\left[\frac{\partial^2}{\partial t^2}(\boldsymbol{A}_e + \boldsymbol{A}_d) + \nabla\left(\Psi_e^e + \Psi_d^e\right) + \nabla\times\left(\frac{1}{\epsilon_e}\frac{\partial \boldsymbol{F}_e}{\partial t} + \frac{1}{\epsilon_d}\frac{\partial \boldsymbol{F}_d}{\partial t}\right)\right]_{\tan} = \left[\frac{\partial \boldsymbol{E}^i}{\partial t}\right]_{\tan} \quad (17)$$

$$\left[\frac{\partial^2}{\partial t^2}(\boldsymbol{F}_e + \boldsymbol{F}_d) + \nabla\left(\Psi_e^m + \Psi_d^m\right) - \nabla\times\left(\frac{1}{\mu_e}\frac{\partial \boldsymbol{A}_e}{\partial t} + \frac{1}{\mu_d}\frac{\partial \boldsymbol{A}_d}{\partial t}\right)\right]_{\tan} = \left[\frac{\partial \boldsymbol{H}^i}{\partial t}\right]_{\tan}. \quad (18)$$

The integrals (17) and (18) are then solved by discretizing the body using triangular patches and with the use of Rao–Wilton–Glisson (RWG) basis functions [6]. Details of the numerical solution are described in [7]. Also, note that for the case of perfectly conducting bodies, the equivalent magnetic currents are zero and we solve (17) for the external region only [8].

III. Formulation of FDTD-PML

The FDTD method uses a system of finite-difference equations for representing the Maxwell's partial differential equations given by

$$\nabla\times\mathbf{E} = -\frac{\partial \mathbf{B}}{\partial t} - \mathbf{J}_m \quad (19)$$

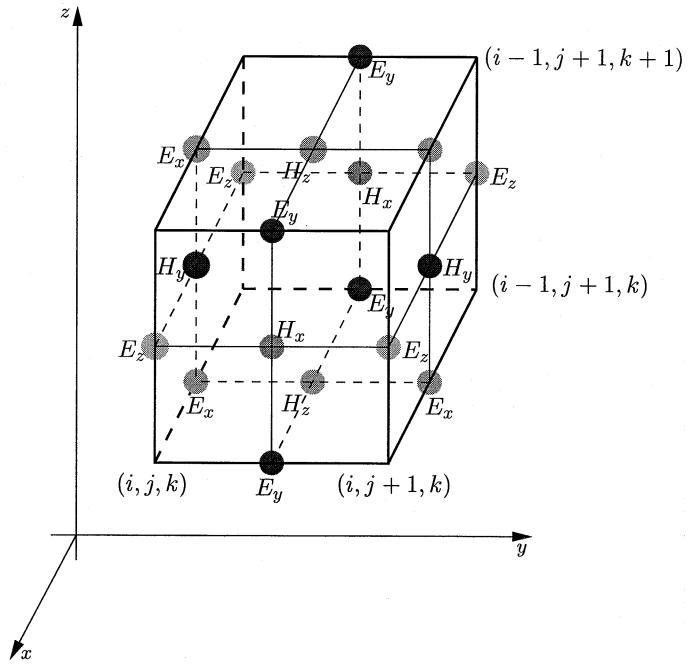

Fig. 1. Interleaving of the electric and magnetic field components at the nodes on a unit cube cell of the space lattice.

$$\nabla\times\mathbf{H} = \frac{\partial \mathbf{D}}{\partial t} + \mathbf{J}_e \quad (20)$$

$$\nabla\cdot\mathbf{D} = \rho \quad (21)$$

$$\nabla\cdot\mathbf{B} = 0. \quad (22)$$

The finite-difference approximation to any derivative of a function is obtained from the Taylor's series expansion of the function. Normally, the central difference approximation is used because the error for the central difference approximation is of second order. In Yee's method [9] of FDTD calculation, the electric and magnetic field components are interleaved in space and time so as to permit a natural satisfaction of the continuity of the tangential field components at the media interfaces. The Yee's Cell is shown in Fig. 1.

Yee's algorithm is implemented by discretizing the object in the Cartesian domain [Fig. 1]. The temporal update scheme of one of the components of the electric (**E**) and magnetic (**H**) fields using Yee's algorithm is given by, (23-24) at the bottom of the next page, where, $\triangle x$, $\triangle y$, and $\triangle z$ are the spatial steps and $\triangle t$ is the time step and ϵ, μ, σ, and $\sigma^\star$ are the permittivity, permeability, electrical, and magnetic conductivities, respectively. Other components of the fields may be written in a similar way.

As the Maxwell's equations are hyperbolic in nature, the FDTD is unbounded in one or more of the spatial directions. Thus, to terminate the computational domain, a boundary condition has to be applied. The most popularly used boundary condition is the PML. The scattered field FDTD algorithm with PML boundary has been used for computing the electromagnetic interactions presented in this paper.

There are two sources of reflections from the PML boundary. The first is the perfectly conducting conditions terminating the PML. As the outward propagating wave passes through the PML, it gets absorbed. However, on reaching the perfectly conducting medium terminating the PML, it gets reflected back

toward the computational domain which may interfere with the scattered fields. This may be reduced by increasing the thickness of the PML region and by changing the conductivity profile. The other source of reflection is the first layer of the PML. At this layer, the matching impedance condition cannot be met as the magnetic conductivity is zero. This is because of the half-spatial step difference between the electric and magnetic parameters used in the FDTD. This may be minimized by choosing a small value for the electric conductivity of the first layer and increasing logarithmically along the layers. Thus

$$\sigma(\rho) = \sigma(0)\left(g^{1/\triangle}\right)^{\rho}$$

where, $\sigma(\rho)$ is the conductivity profile, ρ is the distance from the vacuum-PML interface, and $\sigma(0)$ is the conductivity in the first vacuum-PML interface. $\triangle$ is either, $\triangle x$, or $\triangle y$, or $\triangle z$, and g is the geometric progression ratio of the conductivity, from one cell to the next. The value of g is calculated based on the number of discretization points on the object in a given direction, N_S. Further

$$\log_{10}(g) = \alpha + \beta\,\log_{10}(N_S) + \gamma\,[\log_{10}(N_S)]^2 \qquad (25)$$

where, α, β, and γ are coefficients. Also, $\alpha = 1.7842$, $\beta = -1.0433$, and $\gamma = 0.17749$, for a late time-ripple error of 3%; or $\alpha = 1.5851$, $\beta = -1.0156$, and $\gamma = 0.18495$ for an error of 1% [4]. In this work, the latter set of values of α, β, and γ have been used to attain the lower-ripple error. The value of g obtained from (25) is used to calculate the number of PML layers, along a given direction, using the following expression

$$N = \frac{1}{\ln(g)}\ln\left\{1 - \frac{c}{4\pi}(\sqrt{g}-1)\ln[R(0)]\frac{\Theta}{\triangle}D_c\right\} \qquad (26)$$

here, $R(0)$ is the reflection factor for normal incidence. An optimum value of $R(0)$ is 0.01. D_c is the total duration of the computation in seconds and Θ is a multiplying factor which has been optimally found to be 10 [4]. The variation of the reflection coefficient for any other angle of incidence θ with respect to the normal, is given by

$$R(\theta) = [R(0)]^{\cos\theta}.$$

To calculate the far field, the electric and the magnetic surface currents are calculated on virtual cubes surrounding the object. The cube, on which the electric surface current is calculated, is located at a distance of half the spatial discretization from each of the extremum points of the object along the coordinate axes. The cube for the magnetic surface currents, is located at the extremum points of the object. The electric and magnetic currents are calculated using

$$\mathbf{J} = \widehat{n}\times(\mathbf{H}^s + \mathbf{H}^i), \text{ and } \mathbf{M} = -\widehat{n}\times(\mathbf{E}^s + \mathbf{E}^i) \qquad (27)$$

respectively. Here, $\mathbf{E}^s$ and $\mathbf{H}^s$ are the scattered electric and magnetic fields, respectively, $\mathbf{E}^i$ and $\mathbf{H}^i$ are incident electric and magnetic fields, respectively, and, $\widehat{n}$ is the unit outward normal to the virtual surfaces comprising the cube. Using these

$$\begin{aligned} E_n^x\left(i+\frac{1}{2},j,k\right) &= \left[\frac{\epsilon(i+\frac{1}{2},j,k)}{\epsilon(i+\frac{1}{2},j,k)+\sigma(i+\frac{1}{2},j,k)\Delta t}\right] \\ &\quad\times E_x^{n-1}\left(i+\frac{1}{2},j,k\right) \\ &\quad+\left[\frac{\Delta t}{\epsilon(i+\frac{1}{2},j,k)+\sigma(i+\frac{1}{2},j,k)\Delta t}\right] \\ &\quad\times\left[\frac{H_z^{n-1/2}(i+\frac{1}{2},j+\frac{1}{2},k)-H_z^{n-1/2}(i+\frac{1}{2},j-\frac{1}{2},k)}{\Delta y}\right. \\ &\quad\left.-\frac{H_y^{n-1/2}(i+\frac{1}{2},j,k+\frac{1}{2})-H_y^{n-1/2}(i+\frac{1}{2},j,k-\frac{1}{2})}{\Delta z}\right] \end{aligned} \qquad (23)$$

$$\begin{aligned} H_x^{n+1/2}\left(i,j+\frac{1}{2},k+\frac{1}{2}\right) &= \left[\frac{\mu\left(i,j+\frac{1}{2},k+\frac{1}{2}\right)}{\mu\left(i,j+\frac{1}{2},k+\frac{1}{2}\right)+\sigma^*\left(i,j+\frac{1}{2},k+\frac{1}{2}\right)\Delta t}\right] \\ &\quad\times H_x^{n-1/2}\left(i,j+\frac{1}{2},k+\frac{1}{2}\right) \\ &\quad+\left[\frac{\Delta t}{\mu\left(i,j+\frac{1}{2},k+\frac{1}{2}\right)+\sigma^*\left(i,j+\frac{1}{2},k+\frac{1}{2}\right)\Delta t}\right] \\ &\quad\times\left[\frac{E_y^n\left(i,j+\frac{1}{2},k+1\right)-E_y^n\left(i,j+\frac{1}{2},k\right)}{\Delta z}\right. \\ &\quad\left.-\frac{E_z^n\left(i,j+1,k,\frac{1}{2}\right)-E_z^n\left(i,j,k+\frac{1}{2}\right)}{\Delta y}\right] \end{aligned} \qquad (24)$$

currents, the electric and magnetic vector potentials are calculated using (5) and (6). From these vector potentials the far field is obtained.

IV. Numerical Results

In this section, we present numerical results for a cube and a sphere, both conducting and dielectric materials, obtained by FDTD-PML and TDIE. Note that the TDIE solution has already been compared well with the frequency domain solution for the cube problem [6] and Mie series solution [5] for the sphere problem. Thus, in this work we use TDIE solution as the bench mark and compare the FDTD solution to check the accuracy.

The objects are illuminated by a Gaussian plane wave given by

$$\mathbf{E}^i(\mathbf{r},t) = \mathbf{E}_o \frac{4.0}{T\sqrt{\pi}} e^{-\left[4.0/T\,(ct-ct_o-\mathbf{r}\cdot\hat{\mathbf{k}})\right]^2} \tag{28}$$

where, $\mathbf{E}^i$ is the incident electric field, $\mathbf{r}$ is the position vector of the observation point, $\hat{\mathbf{k}}$ is the unit vector in the direction of propagation of the incident wave, T is the pulse width of the Gaussian impulse, $\mathbf{E}_o \cdot \hat{\mathbf{k}} = 0$, t_o is a time delay that represents the time at which the pulse peaks at the origin, and, c is the velocity of propagation of the electromagnetic wave.

The pulse-width T is defined such that for $ct - ct_o - \mathbf{r}\cdot\hat{\mathbf{k}} = \pm T/2$ the exponential has fallen to about 2% of its peak. For all the cases presented in this work, $\mathbf{E}_o = 377.0\,\hat{\mathbf{a}}_x$, $\hat{\mathbf{k}} = -\hat{\mathbf{a}}_z$, $T = 4.0\ \ell$m (light-meter), and $ct_o = 6.0\ \ell$m. Note, that $1\ \ell\text{m} = 1/3.0 \times 10^8$ s is the time taken by the electromagnetic wave to travel a distance of 1.0 m in free space. Lastly, we note that for the FDTD case, the time step Δt is chosen using the following criterion, given by

$$v\Delta t = 0.7 \times \left[\frac{1}{\Delta x^2} + \frac{1}{\Delta y^2} + \frac{1}{\Delta z^2}\right]^{-1/2}$$

where v is the velocity of the electromagnetic wave in free space and in dielectric media for conducting and material bodies, resepctively.

As a first example, let us consider a conducting cube. The cube is the easiest geometry to solve via the FDTD-PML because it conforms well to the Cartesian grid. Fig. 2 shows the back-scattered field ($\theta = 0°$, $\phi = 0°$) and the side-scattered field ($\theta = 90°$, $\phi = 90°$) for a cube of side length 1.0 m. The FDTD-PML space extends to 1.9 m from the origin along x, y, and z directions and is divided into 38 equal divisions. This results in 534 342 unknowns. For the TDIE solution, the surface of the cube is divided into 4, 5, and 5 uniform segments, along the x, y, and z directions, respectively. By connecting the diagonals of the resulting patches, a total of 260 triangular patches with 390 unknowns were obtained. Note, that for the TDIE solution, the timestep $\Delta t = 0.04717\ \ell$m. However, note that FDTD computations involves interactions between neighboring nodes only, whereas for the TDIE solution, each element is coupled to all other elements. As shown in Fig. 2, the solutions from these two methods agree very well. As for the computer resources are concerned, the TDIE requires around 640 KB storage whereas FDTD-PML requires around 2.0 MB. It may be pointed out that the TDIE solution compares very well with the inverse Fourier-transformed frequency domain solution [8].

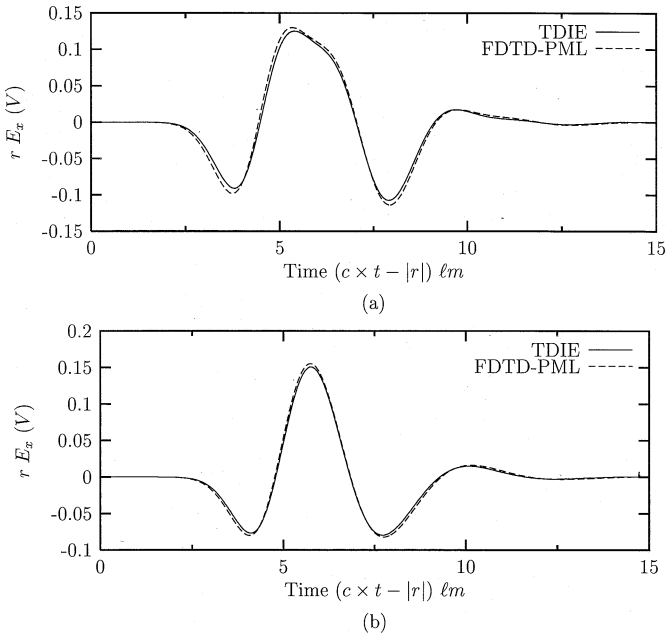

Fig. 2. Far-field response of a conducting cube of side 1.0 m illuminated by a Gaussian plane wave. (a) Back-scattered field ($\theta = 0°$, $\phi = 0°$). (b) Side-scattered field ($\theta = 90°$, $\phi = 90°$).

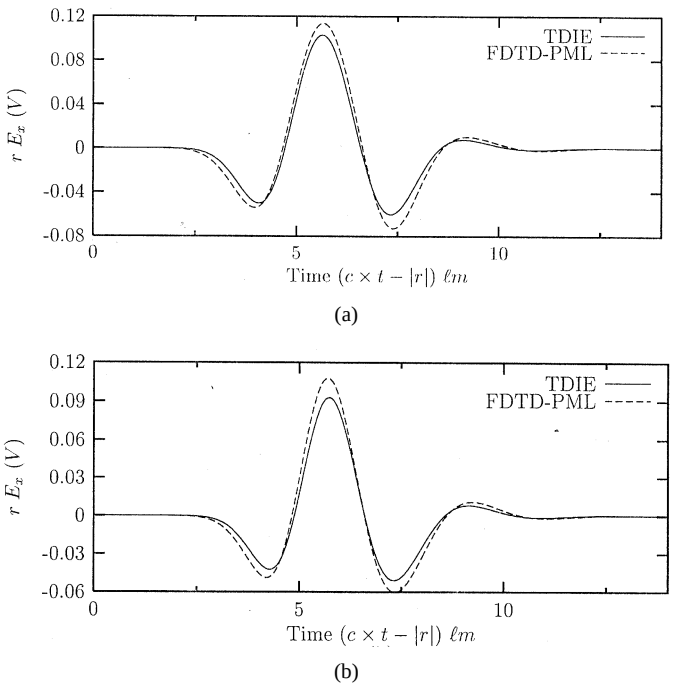

Fig. 3. Far-field response of a conducting sphere of diameter 1.0 m illuminated by a Gaussian plane wave. (a) Back-scattered field ($\theta = 0°$, $\phi = 0°$). (b) Side-scattered field ($\theta = 90°$, $\phi = 90°$).

As a next example, we consider the case of a conducting sphere of diameter 1.0 m. The sphere represents a challenging problem for both the TDIE and FDTD solutions. For the FDTD-PML solution the same grid is used as that of the cube. However, the actual sphere is a stair-stepped approximation. For the TDIE solution, the spherical surface is divided into six divisions along the θ direction. Each ring has (starting from

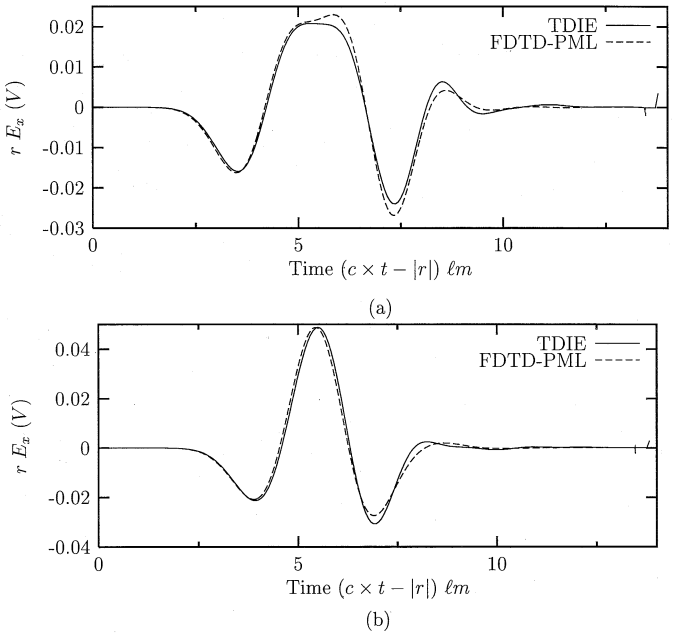

Fig. 4. Far-field response of a dielectric ($\epsilon_r = 2.0$) cube of side 1.0 m illuminated by a Gaussian plane wave (a) Back-scattered field ($\theta = 0°$, $\phi = 0°$) and (b) Side-scattered field ($\theta = 90°$, $\phi = 90°$).

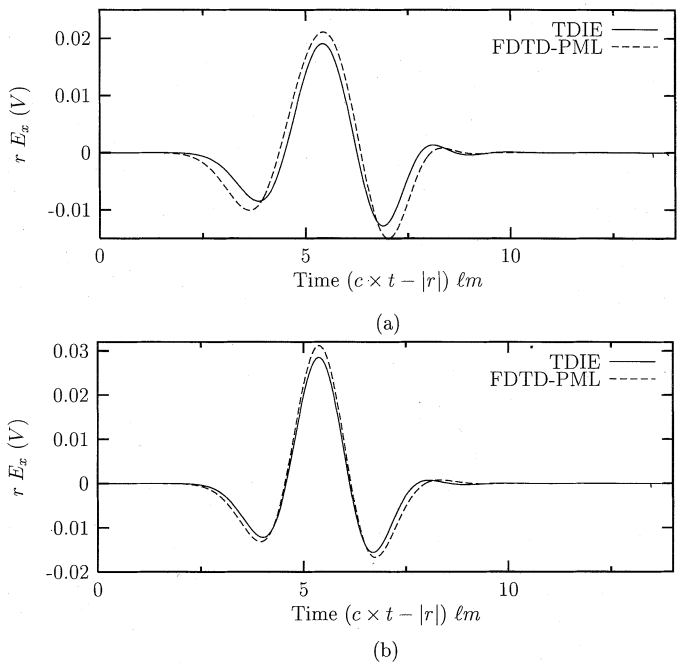

Fig. 5. Far-field response of a dielectric ($\epsilon_r = 2.0$) sphere of diameter 1.0 m illuminated by a Gaussian plane wave. (a) Back-scattered field ($\theta = 0°$, $\phi = 0°$). (b) Side-scattered field ($\theta = 90°$, $\phi = 90°$).

the top) 13, 27, 29, 27, and 13 patches, respectively, for a total of 138 patches and 207 unknowns. This scheme is chosen so that the triangle would be closer to being equilateral. For the TDIE solution, the timestep $\Delta t = 0.07777$ ℓm. The numerical results are presented in Fig. 3. Considering the vast differences in the gridding employed by the numerical techniques, both techniques provide extremely close solutions. The computer resources for the FDTD-PML technique is the same as that for the cube. However, in the case of TDIE the computer storage requirement is around 200 KB.

Next, we consider a dielectric cube of side length 1.0 m and relative permittivity (ϵ_r) 2.0. For this example, the FDTD-PML grid extends to 1.55 m from the origin along x, y, and z directions. This is divided into 62 equal divisions, which results in 2 152 926 unknowns. This amounts to a computer storage of around 8.0 MB. Note, that this discretization amounts to roughly half of the step size for the dielectric problem when compared to conducting case. We opted for this dense discretization to obtain close comparsion with TDIE case, although, the coarse grid scheme provided a reasonable comparison spacifically at the peak values of the pulse. For the TDIE solution the same discretization of the conducting cube is used. However, since magnetic currents are also included, the number of unkowns for the dielectric case are twice compared to that of the corresponding conducting body. Note, that the TDIE solution has to be done only over the scatterer surface. Also, for the TDIE solution, we need to store the magnetic currents on the surface. Together this requires a computer storage of around 3.0 MB. The time step for the dielectric case is the same as that of the conducting cube. Fig. 4 shows the solutions from these two methods, which agree very well. We again note, that the TDIE solution compares very well with the inverse Fourier-transformed frequency domain solution [7].

As the final example, we consider a dielectric sphere, having a relative permittivity of 2.0. The diameter of the sphere is 1.0 m. The FDTD-PML discretization used is the same as that used for the dielectric cube and that for the TDIE is the same as the conducting sphere. The computer storage for TDIE is around 1.0 MB. Fig. 5 shows the results obtained from both methods, which compare very well.

V. Conclusion

In this paper, we compared FDTD-PML and TDIE solutions for certain standard canonical problems. We note that both methods generate reasonably accurate solutions for a given discretization scheme. For the examples considered in the work, it appears that TDIE is more efficient. However, the inference may not be valid for more complex bodies, particularly when dealing with multiple or inhomogeneous materials. Finally, we conclude that these two methods may be used concurrently to check one result against the other.

References

[1] A. Taflove, *Computational Electrodynamics: The Finite-Difference Time-Domain Method*. Boston, MA: Artech House, 1995.

[2] S. M. Rao, Ed., *Time Domain Electromagnetics*. New York: Academic, 1999.

[3] J.-P. Bérenger, "Three-dimensional perfectly matched layer for the absorption of electromagnetic waves," *J. Comput. Phys.*, vol. 127, pp. 363–379, 1996.

[4] ——, "Perfectly matched layer for the FDTD solution of wave-structure interaction problems," *IEEE Trans. Antennas Propagat.*, vol. 44, pp. 110–117, Jan. 1996.

[5] R. F. Harrington, *Time-Harmonic Electromagnetic Fields*. New York: McGraw-Hill, 1961.

[6] S. M. Rao, D. R. Wilton, and A. W. Glisson, "Electromagnetic scattering by surfaces of arbitrary shape," *IEEE Trans. Antennas Propagat.*, vol. 30, pp. 409–418, May 1982.

[7] D. A. Vechinski, S. M. Rao, and T. K. Sarkar, "Transient scattering from three-dimensional arbitrarily shaped dielectric bodies," *J. Opt. Soc. Amer.*, vol. 11, pp. 1458–1470, 1994.
[8] D. A. Vechinski and S. M. Rao, "A stable procedure to calculate the transient scattering by conducting surfaces of arbitrary shape," *IEEE Trans. Antennas Propagat.*, vol. 40, pp. 661–665, June 1992.
[9] K. S. Yee, "Numerical solution of initial boundary value problems involving Maxwell's equations in isotropic media," *IEEE Trans. Antennas Propagat.*, vol. 14, pp. 302–307, May 1966.

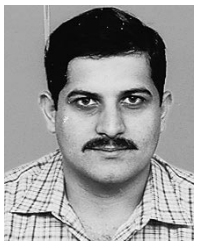

Niraj Sachdeva received the B.E. degree in electronics from Bangalore University, Bangalore, India, and the M.Sc.(Eng.) degree from the Indian Institute of Science, Bangalore, India, in 1990 and 1993, respectively.

In 1993, he joined the Indian Institute of Science, Department of Aerospace Engineering Computational Electromagnetics Group, as a Research Scholar, where he also became a Project Associate while working toward the Ph.D. degree. His research topic was the application of finite difference time domain method for target identification problems. Unfortunately, although his Ph.D. thesis was ready for submission, he lost his life in a road accident in June 2000.

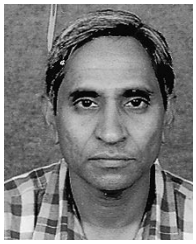

Sadasiva M. Rao (M'83–SM'90–F'00) received the B.E. degree in electrical communication engineering from Osmania University, Andra Pradesh, India, the M.E. degree in microwave engineering from the Indian Institute of Sciences, Bangalore, India, and the Ph.D. degree in electromagnetic theory, University of Mississippi, Oxford, MS, in 1974, 1976, and 1980, respectively.

From 1980 to 1985, he was an Assistant Professor with the Rochester Institute of Technology, Department of Electrical Engineering. From 1985 to 1987, he was a Senior Scientist at Osmania University. From 1987 to 1988, he was a Visiting Associate Professor in the Department of Electrical Engineering, University of Houston, Houston, TX. Since 1988, he has been a Professor in the Department of Electrical Engineering, Auburn University, Auburn, AL. He has worked extensively in the area of numerical modeling techniques as applied to Electromagnetic Scattering. He and his team were the original researchers to develop the planar triangular patch model and to solve the problem of electromagnetic scattering by arbitrary shaped conducting bodies, at the University of Mississippi. He has published well over 100 papers in international journals and conferences. His research interests include numerical methods applied to antennas and scattering.

Dr. Rao received the Best Paper Award from SUMMA Foundation from 1979 to 1981.

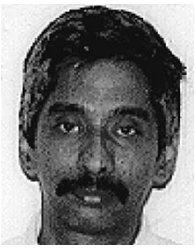

N. Balakrishnan received the B.E. degree (Hons.) in electronics and communication from the University of Madras, Chëpaük, Chënnai, South India, and the Ph.D. degree from the Indian Institute of Science, Bangalore, India, in 1972 and 1979, respectively.

He is currently a Professor in the Department of Aerospace Engineering, Indian Institute of Science and Chairman of the Division of Information Sciences and Services. He has made significant contributions to the creation of the Center for Microprocessor Applications, the National Center for Science Information, and the Supercomputer Education and Research Center, Indian Institute of Science. He has been a Visiting Professor with the Carnegie Mellon University, the National Severe Storms Laboratory, Norman, OK, the University of Oklahoma, Norman, and Colorado State University. He has over 150 publications in international journals and conferences, including numerical electromagnetics, polarimetric radars, information and network security, speech processing, and aerospace electronic systems. He is a consultant to several defence and governmental agencies.

Dr. Balakrishnan is a Fellow of all the major Science and Engineering Academies in India, and a Member of the Scientific Advisory Committee to the Cabinet (SAC-C) to the Government of India. He is the Editor of *Electromagnetics, International Journal of Computational Science and Engineering* and the *Journal of IETE*. He is an Honorary Professor in JNCASR and NIAS. He is the recipient of numerous awards including the Alumni Award for Excellence in Research, the Science and Engineering Award by IISc 2001, Jawaharlal Nehru Centenary Lecturership Award, 2001, the Millennium Medal, 2000, Hari Om Ashram Prerit Dr. Vikram Sarabhai Research Award in 1995, and the J. C. Bose Memorial Award for Best Paper, in 1987 and 2000.